Received: 23 August 2017 | Revised: 31 May 2018 | Accepted: 20 June 2018

DOI: 10.1111/gcb.14395

PRIMARY RESEARCH ARTICLE

WILEY Global Change Biology

Disentangling seasonal and interannual legacies from inferred patterns of forest water and carbon cycling using tree-ring stable isotopes

Paul Szejner[1] | William E. Wright[1] | Soumaya Belmecheri[1] | David Meko[1] | Steven W. Leavitt[1] | James R. Ehleringer[2] | Russell K. Monson[1,3]

[1]Laboratory of Tree-Ring Research, University of Arizona, Tucson, Arizona

[2]Stable Isotope Ratio Facility for Environmental Research, Department of Biology, University of Utah, Salt Lake City, Utah

[3]Department of Ecology and Evolutionary Biology, University of Arizona, Tucson, Arizona

Correspondence
Paul Szejner, Laboratory of Tree-Ring Research, University of Arizona, 1215 E. Lowell Street, Tucson, AZ 85721.
Email: paulszejner@email.arizona.edu

Funding information
Division of Emerging Frontiers, Grant/Award Number: 1065790; Division of Environmental Biology, Grant/Award Number: 1754430; National Science Foundation, Grant/Award Number: 1137336

Abstract

Tree-ring carbon and oxygen isotope ratios have been used to understand past dynamics in forest carbon and water cycling. Recently, this has been possible for different parts of single growing seasons by isolating anatomical sections within individual annual rings. Uncertainties in this approach are associated with correlated climate legacies that can occur at a higher frequency, such as across successive seasons, or a lower frequency, such as across years. The objective of this study was to gain insight into how legacies affect cross-correlation in the $\delta^{13}C$ and $\delta^{18}O$ isotope ratios in the earlywood (EW) and latewood (LW) fractions of *Pinus ponderosa* trees at thirteen sites across a latitudinal gradient influenced by the North American Monsoon (NAM) climate system. We observed that $\delta^{13}C$ from EW and LW has significant positive cross-correlations at most sites, whereas EW and LW $\delta^{18}O$ values were cross-correlated at about half the sites. Using combined statistical and mechanistic models, we show that cross-correlations in both $\delta^{13}C$ and $\delta^{18}O$ can be largely explained by a low-frequency (multiple-year) mode that may be associated with long-term climate change. We isolated, and statistically removed, the low-frequency correlation, which resulted in greater geographical differentiation of the EW and LW isotope signals. The remaining higher-frequency (seasonal) cross-correlations between EW and LW isotope ratios were explored using a mechanistic isotope fractionation–climate model. This showed that lower atmospheric vapor pressure deficits associated with monsoon rain increase the EW-LW differentiation for both $\delta^{13}C$ and $\delta^{18}O$ at southern sites, compared to northern sites. Our results support the hypothesis that dominantly unimodal precipitation regimes, such as near the northern boundary of the NAM, are more likely to foster cross-correlations in the isotope signals of EW and LW, potentially due to greater sharing of common carbohydrate and soil water resource pools, compared to southerly sites with bimodal precipitation regimes.

KEYWORDS

cross-correlation, drought, high-resolution, North American Monsoon, paleoclimatology, precipitation, stable isotopes, vapor pressure deficit

1 | INTRODUCTION

In the western United States, patterns in forest carbon and water cycling are determined by topography and its interaction with precipitation (Schimel et al., 2002; Zapata-Rios, Brooks, Troch, McIntosh, & Rasmussen, 2016). Ecosystem-atmosphere CO_2 exchange in western forests is controlled in large part by the annual delivery of water from the melting winter snowpack (Hu, Moore, Burns, & Monson, 2010; Monson et al., 2005; Winchell, Barnard, Monson, Burns, & Molotch, 2016), while summer rains can compensate for snowpack limitations (Berkelhammer, Stefanescu, Joiner, & Anderson, 2017; West, Hultine, Burtch, & Ehleringer, 2007). Summer rain in the southwestern United States is delivered by the North American Monsoon (NAM), a climate system that has been active during the Holocene (Betancourt, 1990; Bhattacharya, Tierney, & DiNezio, 2017). The utilization of soil water from different seasonal precipitation sources, and the photosynthetic efficiencies that are realized by interannual variation in the amounts of winter and summer precipitation, can be inferred through studies of the carbon and oxygen stable-isotope ratios in the α-cellulose of tree rings (Barbour, Walcroft, & Farquhar, 2002; Craig, 1954; Francey & Farquhar, 1982; Leavitt & Long, 1986; Libby & Pandolfi, 1974).

Most often, tree-ring stable-isotope analysis is used to study interannual and decadal scale relationships between climate and carbon/water cycling (Bale et al., 2011; Leavitt, 2002; Roden & Ehleringer, 2007; Treydte et al., 2007; Wright & Leavitt, 2006). However, more finely resolved temporal-scale analyses, such as those utilizing the earlywood (EW) and latewood (LW) portions of annual rings, have also been used (Babst et al., 2016; Fritts, 1976; Griffin et al., 2013; Kerhoulas, Kolb, & Koch, 2017; Labotka, Grissino-Mayer, Mora, & Johnson, 2016; Leavitt, 2002; Meko & Baisan, 2001; Ogée et al., 2009; Pellizzari, Camarero, Gazol, Sangüesa-Barreda, & Carrer, 2016; Sargeant & Singer, 2016; Szejner et al., 2016; Vaganov et al., 2009; Walcroft, Silvester, Whitehead, & Kelliher, 1997). At the onset of the growing season, cambial activity in conifer stems initiates xylogenesis forming earlywood (EW), which is usually characterized by large-diameter tracheids. As the early growing season progresses into summer, cambial activity slows, producing a distinguishable change in ring anatomy characterized by smaller-diameter tracheids with thicker cell walls and smaller lumens, giving the wood a darker hue, which is known as latewood (LW) (Pallardy, 2008). These anatomical features and seasonal differences between EW and LW should reflect phenological processes cued to photoperiod and temperature, as well as the direct influences of a changing seasonal climate on carbon and water availability. The stable-isotope composition of cellulose in these different tissues records fractionations associated with both kinetic and thermodynamic (equilibrium) influences on carbon and water exchanges through the soil–plant–atmosphere continuum (Farquhar, Cernusak, & Barnes, 2007; Farquhar, Ehleringer, & Hubick, 1989; Roden, Lin, & Ehleringer, 2000).

According to theory, the relative influences of stomatal conductance (g_s) and photosynthetic carbon assimilation rate (A) will determine the gradient between the intercellular (c_i) to ambient (c_a) CO_2 concentrations. Ignoring the mesophyll conductance and associated mesophyll CO_2 concentration for simplicity, diffusive fractionation at the leaf surface, the c_i/c_a ratio and biochemical fractionation during photosynthesis, together, can be used to approximate the diffusive and metabolic isotope effects driving ^{13}C discrimination (Ehleringer & Cerling, 1995; Farquhar, Oleary, & Berry, 1982). Examination of the $\delta^{13}C$ in cellulose allows for physiological inferences about the molar intrinsic leaf water-use efficiency (iWUE = A/g_s) and its relation to climate variability through time (Farquhar et al., 1982; Francey & Farquhar, 1982; Frank et al., 2015; Gessler et al., 2014; Leavitt, 2001; Roden & Ehleringer, 2007). The oxygen stable-isotope ratios in wood cellulose ($\delta^{18}O$) are influenced by two main variables: temporal variability in the isotopic content of the water sources used by plants and isotopic enrichment (in transpiring leaves) driven by the atmospheric vapor pressure deficit (VPD) (Roden et al., 2000; Treydte et al., 2014). When the isotopic content of the water source is known, it is possible to isolate the isotopic enrichment component of discrimination (e.g., $\Delta^{18}O$) which is driven by atmospheric VPD and recorded in wood cellulose (Barbour et al., 2002; Cernusak et al., 2016; Farquhar et al., 1993). One challenge, however, with climatic interpretation of isotope ratios in EW and LW, is that these ratios can reflect environmental input from multiple seasons and past years, consequently blurring the differences caused by specific seasonal climate regimes (Gessler et al., 2014; Helle & Schleser, 2004; Szejner et al., 2016; Vaganov et al., 2009). The cross-correlation between isotope ratios in EW and LW has been observed previously (Helle & Schleser, 2004; Kagawa, Sugimoto, & Maximov, 2006; Kimak & Leuenberger, 2015; Kress et al., 2009; Leavitt, 2002; Vaganov et al., 2009). This correlation can be attributed to external (e.g., persistent interannual climate trends) and internal (e.g., mixing of carbon and water pools) processes, and the assessment of the relative importance of these influences will provide insights into how to better read the seasonal and interannual alignment of climate-isotope relations.

The geographic domain for our studies was that of the North American Monsoon (NAM) climate system in the southwestern United States (Higgins, Yao, & Wang, 1997; Sheppard, Comrie, Packin, Angersbach, & Hughes, 2002). Past studies on carbon and oxygen isotopes in earlywood (EW) and latewood (LW) of *Pinus ponderosa* (Douglas ex C. Lawson) suggest that forests in the southern part of the study area function, on average, with lower iWUE, than in the northern part, and show lower evaporative enrichment of ^{18}O in LW compared with EW (Szejner et al., 2016). Unresolved, however, was the causal influence of cross-correlation between the isotope ratios of EW and LW, which may obscure otherwise clear signals of seasonal climate variations in some parts of the regional gradient more than others (Kimak & Leuenberger, 2015; Rahman et al., 2016). In this study, we assessed the seasonal and interannual influences on EW and LW isotope ratios using regression models (Griffin et al., 2013; Meko & Baisan, 2001; Stahle et al., 2009; Torbenson, Stahle, Villanueva Díaz, Cook, & Griffin, 2016), and a coupled stable-isotope fractionation–climate model (Barbour, Roden, Farquhar, & Ehleringer, 2004; Roden, Kahmen, Buchmann, & Siegwolf, 2015; Roden et al.,

2000). We addressed three questions: (a) Are seasonally resolved climate-isotope relationships obscured by cross-correlations in the $\delta^{13}C$ and $\delta^{18}O$ ratios between EW and LW? (b) Are there geographical patterns in the cross-correlations between the isotope compositions in EW and LW? (c) Can stable-isotope process models, applied to tree rings, explain temporal and geographic patterns in the dependence of isotope ratios in EW and LW on seasonal climate variation?

2 | MATERIALS AND METHODS

2.1 | Study area

Summer climate across much of the southwestern United States is characterized by an annual monsoon system, the North American Monsoon (NAM). Within the domain of the NAM, winter precipitation decreases from northwest to southeast and summer precipitation decreases from south to north. Within the part of the NAM domain that we studied, the northernmost site (in Utah) receives 20%–30% of the total annual precipitation as summer rain, whereas the southernmost sites (in Arizona and New Mexico) receive 40%–60% of the annual total as summer rain (Figure 1a). Precipitation seasonality is coupled with large variations in atmospheric water vapor pressure deficit VPD (Figure 1c,d). The transition from spring to summer is evident as increased temperature, which results in drier atmospheric conditions during summer—higher VPD—at many locations within the central and northern parts of the region (Figure 1c,d) However, in parts of the southern region—close to the border with Mexico—VPD decreases in summer due to monsoon humidity.

2.2 | Data collection

An updated version of the *Pinus ponderosa* tree-ring isotope network that was originally assembled by Szejner et al. (2016) was used in this study. The new dataset contains two more sites: Bryce Canyon, Utah (BRY, 1960–2015) and Mesa Verde, Colorado (MVP, 1911–2015). Additionally, three chronologies (RCP, LMP, and WCP) were extended back in time from 1960 to the 1930s, and the "common period" used in comparing all sites is 1960–2012. For each site, we developed EW and LW chronologies of both carbon ($\delta^{13}C$) and oxygen ($\delta^{18}O$) isotope ratios, for a total of 52 stable-isotope chronologies from 13 sites (four chronologies per site). The sites are distributed across the southwestern United States with five sites located in Arizona, four sites in New Mexico, three sites in Utah, and one site in Colorado (Figure 1a). At the local scale, we avoided choosing sites with large surrounding watersheds that could contribute runoff water from higher elevations, evidence of past century land-use changes, and evidence of tree-to-tree canopy competition.

We collected 2–3 cores from 20 to 30 trees using 5 mm increment borers. In order to secure enough wood for isotope analysis,

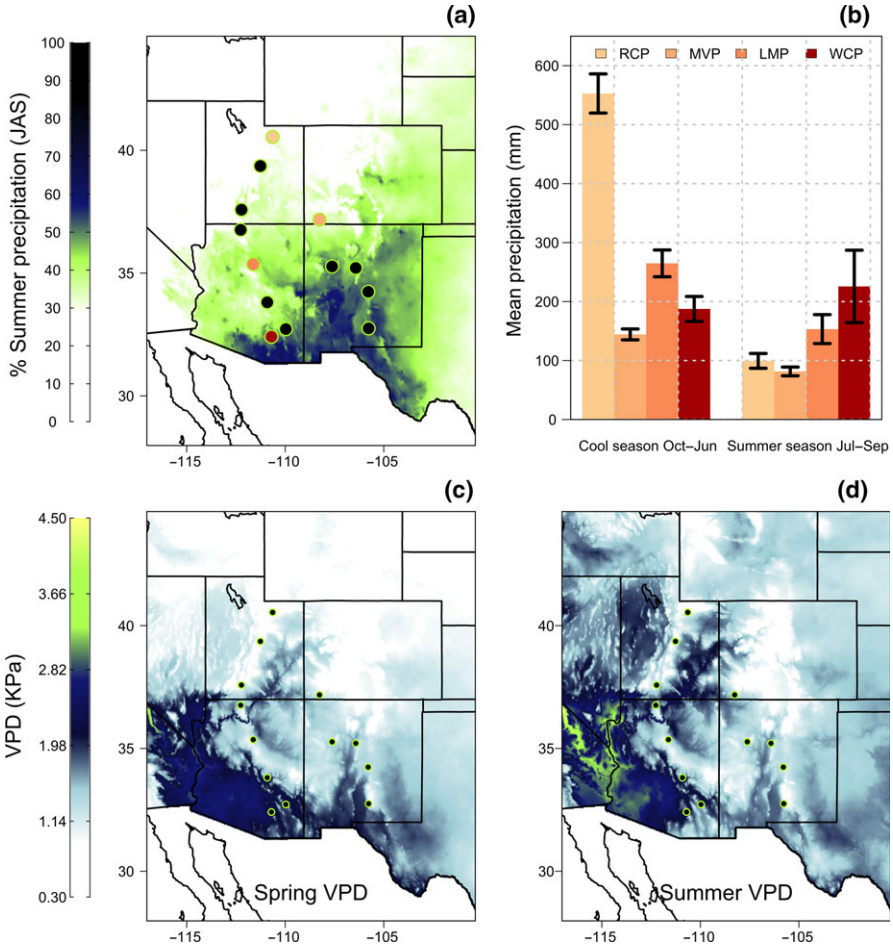

FIGURE 1 Tree-ring network and seasonal moisture regime. Solid dots indicate the thirteen investigated sites. (a) Map of summer precipitation (July, August, September) proportion of annual precipitation in the region of influence of the North American Monsoon (NAM). (b) Mean cool-season (October–September) and summer precipitation at four separate tree-ring sites. Error bars are two standard errors of the mean. (c) Mean spring (AMJ) atmospheric vapor pressure deficit (VPD), (d) mean summer (JAS) VPD. Seasonal changes in VPD with the onset of the summer monsoon in July are an important determinant of leaf carbon and isotope ratios. Monthly data for the period 1895–2015 were obtained from PRISM (PRISM Climate Group, 2004)

we chose 4–5 sampled trees at each site to be processed and further analyzed (Leavitt, 2002; Leavitt & Long, 1986). The trees we analyzed satisfied the following criteria: (a) medium age of ca. 100–150 years, (b) signs of vigorous recent growth with a well-formed and symmetrical crown, and (c) no obvious occurrence of intra-annual density fluctuations (false rings), which complicate the seasonal interpretation of EW and LW formation.

2.3 | Sample preparation and isotope analysis

Samples were mounted using water-soluble hide glue and sanded with fine-grained sand-paper, to allow for visual cross-dating (Stokes & Smiley, 1996). After cross-dating, each dated annual tree ring was sliced into three sections: earlywood (EW), which was split into two halves EW1 and EW2, and latewood (LW) (Figure 2). Samples were ground to 20 mesh—0.84-mm size particles—and heat sealed in permeable bags produced from a polymer fabric (Ankom Technology, Macedon, NY, USA). Samples of α-cellulose were extracted from each wood sample following the method described by Leavitt and Danzer (1993), with the addition of a sodium hydroxide step, and additional modifications as described in Szejner et al. (2016). Only EW1 and LW were used for the isotopic analysis to ensure good seasonal separation of isotope signals. Our initial assumption was that the EW1 division was matured using precipitation from winter and spring and that the LW division was matured using summer precipitation (Belmecheri, Wright, Szejner, Morino, & Monson, 2018; Pallardy, 2008; Szejner et al., 2016; Ziaco, Truettner, Biondi, & Bullock, 2018). For each year and for each site, each subdivision was pooled from all trees into one combined sample, except every 10 years when we analyzed trees separately to quantify intertree variability. The coefficient of variation among trees in each site was low, with averages of: 3.1 ± 0.7% for EW1 $\delta^{13}C$, 4.0 ± 1.2% for LW $\delta^{13}C$, 5 ± 1.6% for EW1 $\delta^{18}O$, and 5.5 ± 3.0% for LW $\delta^{18}O$.

The ratios of $^{13}C/^{12}C$ were measured from the CO_2 produced during α-cellulose combustion in a high-temperature conversion elemental analyzer coupled with a Thermo Delta Isotope Ratio Mass Spectrometer (TC/EA–IRMS) in the Environmental Isotope Laboratory of the Department of Geosciences at the University of Arizona. The $^{18}O/^{16}O$ ratios were measured on the CO produced by α-cellulose pyrolysis (Saurer, Robertson, Siegwolf, & Leuenberger, 1998) in a TC/EA–IRMS at the Stable Isotope Ratio Facility for Environmental Research at the University of Utah. Isotope ratios are expressed in delta (δ) notation relative to the $\delta^{13}C$ VPDB (‰) and $\delta^{18}O$ VSMOW (‰). The $\delta^{13}C$ sample precision was ±0.09‰ (standard deviation calculated from the average difference between measured internal standards, n = 397), and the $\delta^{18}O$ sample precision was ±0.23‰ (n = 570). Each $\delta^{13}C$ chronology was corrected for both decreases in the time-dependent atmospheric $^{13}C/^{12}C$ due to progressive fossil fuel combustion (the so-called Suess effect; Suess, 1955;) and for the influence of progressive increases in atmospheric CO_2 on direct and indirect changes in c_i/c_a, concentration through the so-called preindustrial (PIN) correction (McCarroll et al., 2009).

2.4 | Statistical analysis

We used the cross-correlation function (CCF) analysis (Jenkins & Watts, 1968) to assess the lagged correlation between LW isotope ratios and EW1 isotope ratios. In our case, the CCF is the correlation between two separate time series as a function of number of years of offset:

$$x_t \text{ with } y_{t+i}, i = -10:10, \text{when } x_t \text{ is LW and } y_{t+i} \text{ is EW1 in year}_t \quad (1)$$

For example, in this case, LW was fixed in time and EW1 was lagged several time steps (years) from −10 to 10. For each lagged step, the Pearson correlation coefficient was computed to assess the magnitude of the cross-correlation between EW1 and LW. Negative lags were used to explore the LW correlation on past EW1, and positive lags were used to explore the LW influence on future EW1. The CCF with a parameterized lag of 0 tests for a concurrent (same growing season) relationship between EW1 and LW. We note that uncertainty in the CCF is amplified when the individual series are autocorrelated (Yamaguchi, 1986). To circumvent this source of uncertainty, we also examined the CCF after removing autocorrelation from the individual chronologies with a 10th order autoregressive model (AR(10) model). In previous studies, ring width chronologies that had a significant EW-LW relationship have been adjusted using the residuals of a linear regression model using LW and EW producing the adjusted-LW index (LW_{adj}) (Griffin, Meko, Touchan, Leavitt, & Woodhouse, 2011; Meko & Baisan, 2001; Stahle et al., 2009). Therefore, after exploring the CCF's, we followed the same procedure for producing an adjusted-LW index with respect to $\delta^{13}C$ and $\delta^{18}O$.

To test the effect of the linear regression between LW and EW1, we compared both sets of chronologies with and without adjustment, (LW_{adj} and LW) and regressed each against atmospheric VPD for the "early" and "late" seasonal periods of AMJ and JAS. The VPD in kPa was computed for each month by subtracting the actual vapor pressure (e_a) from the saturated vapor pressure (e_s), using maximum and minimum temperatures to estimate e_s (Ficklin & Novick, 2017), and dew-point temperatures to estimate e_a. The data

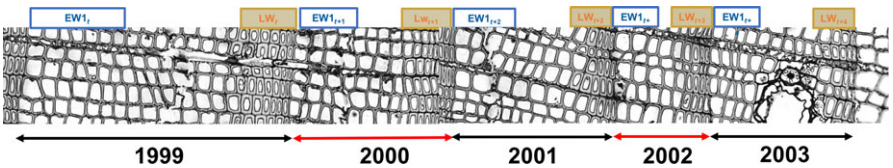

FIGURE 2 Photograph showing the intra-annual sample components of EW1 and LW in annual rings of *Pinus ponderosa* (Image prepared by Kiyomi Morino, University of Arizona)

used for this purpose come from the PRISM dataset (PRISM Climate Group, 2004).

The maximum common temporal variability among the sites was computed using a principal component analysis (PCA) based on the standardized time series of each site (n = 13 and for the 1979–2012 period). We also performed a separate PCA for measurements of $\delta^{18}O$ EW, $\delta^{18}O$ LW_{adj} and for the $\delta^{18}O_{cel}$ and $\Delta^{18}O_{cel}$ modeled for spring and summer (see Supporting Information Appendix S1).

2.5 | Coupled isotope fractionation–climate model of $\delta^{18}O$

We used a forward mechanistic modeling approach to predict the expected oxygen isotope ratios of cellulose at monthly resolution (Barbour et al., 2004; Roden et al., 2000). The model has two main environmental drivers: the isotopic composition of the water sources and atmospheric VPD. The predicted oxygen isotope ratio in cellulose ($\delta^{18}O_{cel}$) is determined as follows (Barbour et al., 2004):

$$\delta^{18}O_{cel} = f_0(\delta^{18}O_{wx} + \varepsilon_c) + (1 - f_0)(\delta^{18}O_{lw} + \varepsilon_c) \quad (2)$$

where $\delta^{18}O_{wx}$ is the isotopic composition of the xylem water (source water), $\delta^{18}O_{lw}$ is the isotopic composition of leaf water that depends on the VPD and the isotopic composition of the water vapor. In deploying this model, we used the $\delta^{18}O$ of the source water to simulate isotopic enrichment in atmospheric water vapor, assuming the isotopic steady-state condition (Craig & Gordon, 1965; Farquhar & Cernusak, 2005) (see Supporting Information Appendix S1). In the model, ε_c, is the average fractionation constant between water and organic material and is taken as ~27‰, despite some evidence indicating that the fractionation can be dependent on temperature (Sternberg & DeNiro, 1983; Sternberg & Ellsworth, 2011). f_0 is the fraction of oxygen atoms exchanged between phloem-transported photosynthate and xylem water (assumed to be source water) during cellulose synthesis; in this case, we used an f_0 = 0.5 due to the aridity of the study region (Cheesman & Cernusak, 2016). The $^{18}O/^{16}O$ of tree-ring cellulose can also be defined in terms of leaf water ^{18}O enrichment above that of source water (Farquhar et al., 1993); this allows for the expression of leaf evaporative enrichment independently from variations in source water isotope ratio (Barbour et al., 2004). This form of the $^{18}O/^{16}O$ ratio is written as $\Delta^{18}O_{cel}$:

$$\Delta^{18}O_{cel} = \Delta^{18}O_{lw}(1 - f_0) + \varepsilon_c \quad (3)$$

To estimate the influence of climate on leaf water enrichment, we used site-specific climate data from the PRISM dataset (PRISM Climate Group, 2004). We estimated the $\Delta^{18}O_{lw}$ following the Craig-Gordon model (see Supporting Information Appendix S1).

We made a simplifying assumption that the xylem water $\delta^{18}O_{wx}$ during the formation of EW is equal to the weighted 3-month moving average $\delta^{18}O$ of winter and spring precipitation ($\delta^{18}O_p$) and the xylem water $\delta^{18}O_{wx}$ during the formation of LW is equal to the monthly mean $\delta^{18}O$ during summer precipitation. The $\delta^{18}O_p$ was computed with the Isotopes-incorporated Global Spectral Model (IsoGSM; Yoshimura, Kanamitsu, Noone, & Oki, 2008), using data at monthly resolution from 1979 to present. For each site, we estimated $\delta^{18}O_p$ from the IsoGSM field using the geospatial coordinates for each field site.

We ran the model for $\delta^{18}O_{cel}$ and $\Delta^{18}O_{cel}$ at a monthly resolution and then calculated 3-month means corresponding to the spring months of April, May, and June (AMJ) and the summer months of July, August, and September (JAS). These months correspond, generally, to the periods of snow melt and monsoon rain, respectively. Modeled isotope ratios were compared with observed measurements of $\delta^{18}O$ in EW1 and LW using two different approaches: (a) comparison of the isotopic mean annual difference between EW1 and LW for measured and modeled $\delta^{18}O$, and (b) comparison of the temporal variability using the first principal component (PC1) of measured and modeled seasonal $\delta^{18}O_{cel}$ and $\Delta^{18}O_{cel}$. In this case, principal component analysis (PCA) allowed us to conduct a heuristic simplification to assess variance in the partitioning of modeled and observed values for $\delta^{18}O_{cel}$ and $\Delta^{18}O_{cel}$ across multiple sites and multiple time series—in essence, evaluating the match between modeled and measured values when expressed to a commonly transformed statistical mode. Taking account of the model's logic, the PCA approach allowed us to assess the differential variance contribution coming from atmospheric demand (VPD, expressed in $\Delta^{18}O_{cel}$) and from the variability of both VPD and the isotopic composition of source water (expressed in $\delta^{18}O_{cel}$).

3 | RESULTS

3.1 | Long-term trends in EW1 and LW

In processing our samples, we routinely made corrections for long-term trends in the atmospheric CO_2 concentration and accompanying responses in c_i/c_a (McCarroll et al., 2009; Suess, 1955). These corrections are commonly applied to tree-ring $\delta^{13}C$ chronologies (Bale et al., 2011;Szymczak, Joachimski, Bräuning, Hetzer, & Kuhlemann, 2012; van der Sleen, Zuidema, & Pons, 2017), with assumptions and procedures based on empirical trends in the state of the atmosphere and theoretical boundaries on the response of c_i/c_a to increases in c_a (McCarroll & Loader, 2004; McCarroll et al., 2009). More recently, an analysis of tree responses to changes in c_a, using over 50 studies in which knowledge or control over c_a was possible, has led to a general prediction of the time-dependent changes in $^{13}C/^{12}C$ fractionation ($\Delta^{13}C$) as c_a changes from ~200 to 400 ppm (Voelker et al., 2016). This analysis showed a nonlinear relationship between $\Delta^{13}C$ to changes in c_a, decreasing from ~0.011‰ per ppm of CO_2 to ~0.006‰ per ppm of CO_2 over the past century (Voelker et al., 2016). This analysis provides a means to assess the spatial and temporal coherence in the time-dependent shifts in our carbon isotope chronologies, against those for numerous tree species responding only to atmospheric changes in $^{13}C/^{12}C$ isotope composition and c_a. We took advantage of the availability of this analysis to further explore possible long-term trends that might be apparent in the $\delta^{13}C$ values of EW1 and LW. Theoretically, divergence in the observed and predicted time series will reveal the degree of spatiotemporal

coherence among multiple sites with regard to isotope responses across multiple decades, and the relative sensitivities of the chronologies to climate versus atmospheric changes in isotope composition and c_a. The results shown in Figure 3 reveal that the thirteen sites investigated show a high degree of spatiotemporal coherence and thus general similarity in the isotope–climate relation observed across a broad geographic domain, and that the procedures that we used to remove atmospheric trends in isotope composition and c_a resulted in clear uncoupling of chronologies from the trend expected for influences of atmospheric composition alone (also see Supporting Information Appendix S1).

3.2 | Temporal dependencies between EW1 and LW

Prior to assessing cross-correlations, we observed that most of the EW1 and LW chronologies of $\delta^{13}C$ and about half of the chronologies of $\delta^{18}O$ are significantly autocorrelated (Figure 4a–d). Significant autocorrelation often extends to a lag of 2 years, meaning that the current year's departure from the mean depends on the departure in the previous 2 years. At some sites, $\delta^{13}C$ EW1 is autocorrelated with a lag of more than 4 years (SLS, KPP, MVP, BRY, and RCP) and $\delta^{13}C$ LW is autocorrelated for more than 2 years (WCP, SLS, SAP, SPP, and MVP). Autocorrelation of $\delta^{18}O$ in EW1 and LW at some sites extends to more than 2 years (WCP, CPP, and RCP). Except for four sites (SAP, GHP, CDT, and MVP), statistically significant autocorrelation was found in $\delta^{13}C$ EW1 and LW chronologies. In the case of $\delta^{18}O$ EW1 and LW chronologies, the northern most sites, in general, did not show autocorrelation with the exception of RCP which is likely explained by a long-term positive trend of $\delta^{13}C$ enrichment, combined with a strong partial autocorrelation of first order (see Supporting Information Appendix S1).

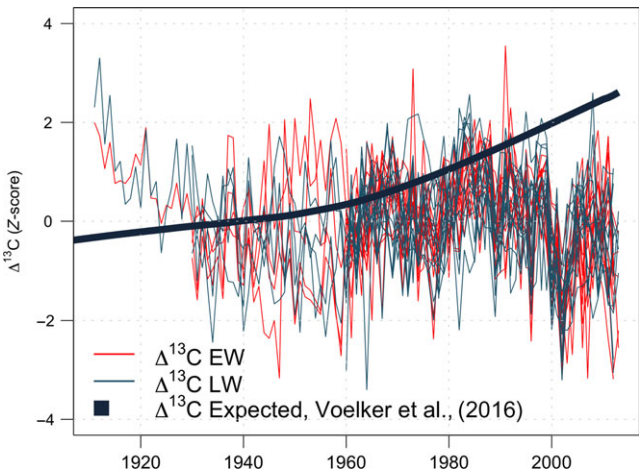

FIGURE 3 Divergent patterns between expected and observed trends in $\Delta^{13}C$. The black line represents the expected $\Delta^{13}C$ considering the effects of increasing the atmospheric CO_2 and Suess effect (Voelker et al., 2016). Red and blue chronologies are the observed $\Delta^{13}C$ (*Z*-scores) for EW and LW, respectively

The relationships among $EW1_{t+0}$ and LW_{t+0} chronologies (lag 0) are statistically significant for most sites. The cross-correlation functions (CCF) of all chronologies suggest that EW1 and LW share a sizeable proportion of the autocorrelation; significant relationships at positive and negative lags occur when LW is correlated with $EW1_{t+i}$. The results shown in Figure 4 support our original hypothesis that common influences are revealed in the isotope ratios of both EW1 and LW, confirming the need to test LW-EW1 relationships without the autocorrelation from each chronology. After applying the autoregressive model of order 10, the residual chronologies called EW1(AR10) and LW(AR10) were used to clarify the lagged relationships that are independent of shared autocorrelation.

After removal of the autocorrelation in each chronology, the relationship between $\delta^{13}C$ $EW1_{t+0}$ and LW_{t+0} remained significant for most sites, except for LMP and SAP. The lagged relationship in SLS, GHP, SPP, KPP, and MFP showed a significant positive relationship between LW and $EW1_{t+1}$, where LW had some statistical influence on EW1 of the following year. In contrast, the $\delta^{18}O$ CCF results showed a significant positive relationship between LW and EW1 of the same year only in some sites SPP, LMP, BRY, KPP, and RCP. At a positive lag of 1 year (LW and $EW1_{t+1}$), only SLS, GHP, CDT, MVP, and BRY showed significant correlations. At a lag of 2 years, some the most southerly sites (SLS and SAP) showed significant correlations between LW and $EW1_{t+2}$.

3.3 | Spatial patterns of EW1-LW connections

The cross-correlation between LW_{t+0} and $EW1_{t+0}$ was significant for most of the $\delta^{13}C$ chronologies, with the exceptions of LMP and SAP (Figures 4 and 5a,b). However, we observed a distinct latitudinal pattern whereby sites in the northerly part of the NAM domain showed a higher EW1-LW correlation compared to the southern sites. For most of the $\delta^{18}O$ chronologies, LW_{t+0} and $EW1_{t+0}$ were independent and with no distinct spatial pattern (Figure 5c). When we analyzed the residual chronologies after the autoregressive (AR10) modeling, we observed a small reduction in the correlation values but no change in the general spatial pattern of the EW1-LW temporal dependence of $\delta^{13}C$ values. However, the correlations between EW1-LW showed a cluster of sites in the southern region where EW1 and LW were statistically independent (Figure 5d).

Because the cross-correlations between EW1 and LW were statistically significant for most of the sites, even after removing the autocorrelation (especially for $\delta^{13}C$; see Figure 5), we used linear regressions between the isotope ratio chronologies in EW1 and LW to obtain the residual chronologies (LW_{adj}) (Griffin et al., 2011; Meko & Baisan, 2001). These residuals (LW_{adj}) are independent from the influence of antecedent conditions, and therefore no significant cross-correlation with EW1. LW_{adj} and LW chronologies were compared with seasonal VPD for AMJ and JAS (Figure 6). As reported in Szejner et al. (2016), LW chronologies were significantly correlated with both spring and summer VPD, whereas most of the LW_{adj} chronologies were significantly correlated only with summer VPD (Figure 6).

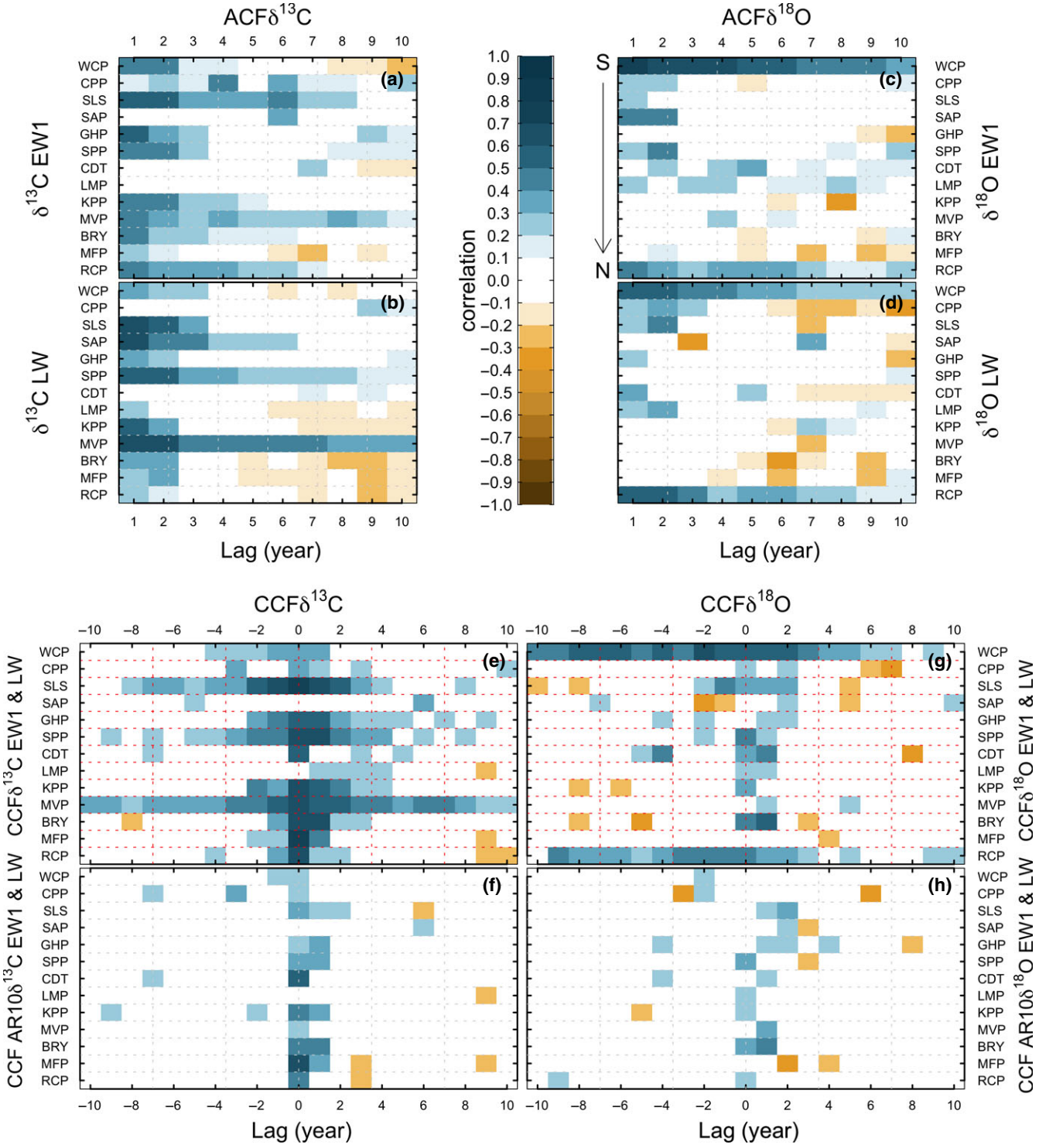

FIGURE 4 Autocorrelation (ACF) and cross-correlation (CCF) summary of the stable-isotope time series. The *x*-axis is lag (years). Tree-ring sites are ordered south to north (top to bottom) along the *y*-axis. Significant ($p < 0.05$) correlations are shown with shaded blue (positive) or brown (negative). The top-half panels show the following ACF results; (a) ACF of EW1 $\delta^{13}C$, (b) ACF of LW $\delta^{13}C$, (c) ACF of EW1 $\delta^{18}O$, and (d) ACF of LW $\delta^{18}O$. The bottom-half panels show the following CCF results; (e) CCF $\delta^{13}C$ using the standard chronologies, (f) CCF $\delta^{13}C$ using the residual chronologies after autoregressive modeling AR(10) (g) CCF $\delta^{18}O$ using the standard chronologies, and (h) CCF $\delta^{18}O$ using the residual chronologies from an AR(10) model

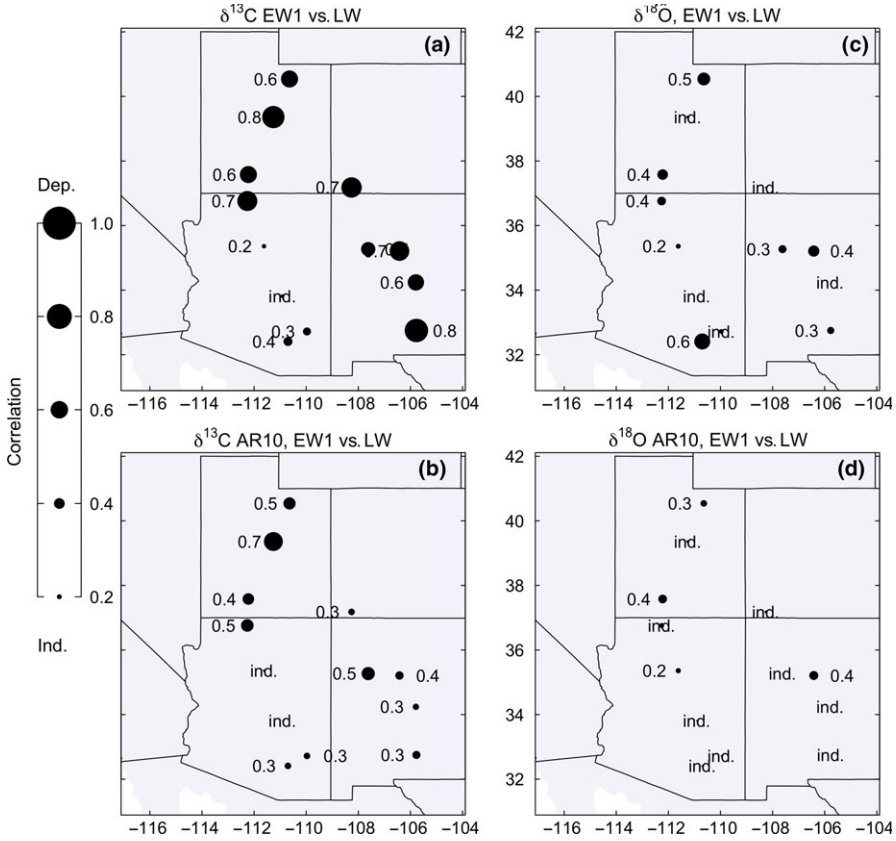

FIGURE 5 EW1-LW correlations after extracting the individual autocorrelation from subannual ring components EW1 and LW. Significant ($p < 0.05$) correlations are shown by the corresponding size of black circles. The original isotope chronologies are shown in the upper maps (a, c) and the AR(10) residual chronologies in the lower maps (b, d). The left side maps are for $\delta^{13}C$, and the right-side maps are for $\delta^{18}O$

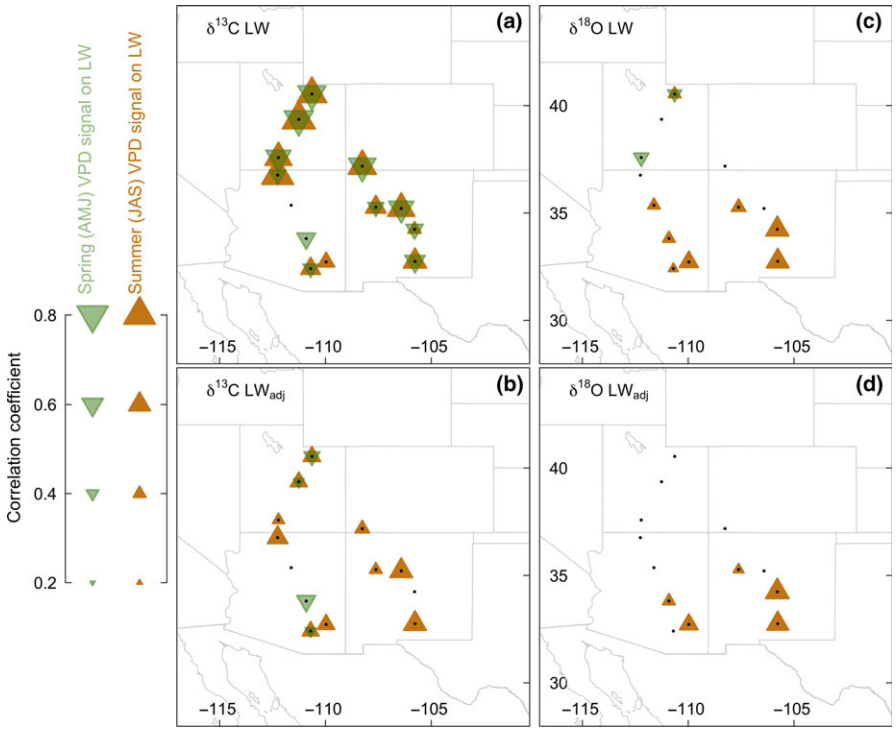

FIGURE 6 Effect of LW adjustment (LW independent from the EW) on the correlation of LW isotope ratios with VPD in spring (AMJ) and summer (JAS). Left panels show results for $\delta^{13}C$ (a, b), and right panels show results for $\delta^{18}O$ (c, d). Top panels are without adjustment of latewood (a, c), and bottom panels are with adjustment (b, d). Correlation and season of climate data are size-coded, and color-coded is according to the left key. Only significant ($p < 0.01$) correlations are coded

3.4 | Coupled isotope fractionation–climate model of $\delta^{18}O$

The EW1 $\delta^{18}O$ was more enriched than the LW $\delta^{18}O$ in the southern sites (~4‰) with the difference decreasing gradually toward the northern sites (~0‰) (Figure 7). These patterns were reproduced using forward mechanistic modeling. When comparing our observations and modeled outputs (Figure 7b), we found an $r^2 = 0.63$ with an RMSE of 1.87‰. The slope of the linear regression between the measured and modeled EW-LW difference revealed an

overestimation of the difference between EW1 and LW, mainly for the southern sites where the modeled difference was larger. Additionally, the temporal variability recorded in the observed PC1 in EW1 is mostly explained by evaporative enrichment (Figure 7c). The temporal variability recorded in the modeled PC1 $\delta^{18}O_{cel}$ modeled for spring (AMJ) did not correlate with observed EW1 $\delta^{18}O$ (Figure 7e). However, the PC1 from $\Delta^{18}O_{cel}$ modeled for spring climate showed significant correlations with the PC1 from EW1 $\delta^{18}O$ (Figure 7c) (see Supporting Information, Table S1). In contrast, the PC1 from both models—$\delta^{18}O_{cel}$ and $\Delta^{18}O_{cel}$—corresponding to summer growth was significantly correlated with the PC1 from LW_{adj} $\delta^{18}O$ (Figure 7d,f). This latter result showed that a significant percentage of the variance was best explained by evaporative enrichment, and another percentage of the variance was most likely explained by the exchange of ^{18}O and ^{16}O between phloem sucrose and nonfractionated source water in the xylem (Sternberg & DeNiro, 1983).

Most of the sites showed a significant, positive correlation between predicted summer $\delta^{18}O$ or $\Delta^{18}O$ and observed LW_{adj} $\delta^{18}O$, reflecting good alignment among monsoon precipitation, summer evaporative enrichment and physiological processes involved in the synthesis of LW_{adj} cellulose (Figure 7g). Six of the seven sites that demonstrated a positive correlation between summer $\delta^{18}O$ and LW_{adj} $\delta^{18}O$ and six of the eight sites demonstrating a positive correlation between summer $\Delta^{18}O$ and LW_{adj} $\delta^{18}O$ are in the southerly part of the studied domain. Only three of the 13 sites demonstrated a significant, positive correlation between spring $\delta^{18}O$ and EW1 $\delta^{18}O$, and two of those are in the northerly part of the studied domain (Figure 7g). Nine of the 13 sites demonstrated a positive correlation between spring $\Delta^{18}O$ and EW1 $\delta^{18}O$, and these were evenly distributed across the latitudinal extent of the studied domain (Figure 7g).

4 | DISCUSSION

An improved understanding of the multiple influences of climate on tree-ring $\delta^{13}C$ and $\delta^{18}O$ from EW and LW is crucial if we want to infer tree water use and carbon assimilation patterns through subannual dendrochronological inference (Belmecheri et al., 2018; Gessler et al., 2014; Treydte et al., 2014). Our aim in conducting this study was to investigate seasonal and interannual lags along a climate gradient as influences on $\delta^{13}C$ and $\delta^{18}O$ in the EW1 and LW tissues within single annual rings. Based on our analysis of *P. ponderosa* trees from 13 sites in the southwestern United States, we documented differences in the autocorrelation structures and the presence of seasonal and interannual lags across the region, influenced annually by the North American Monsoon climate system. Our results provide insight into possible sources of the lag effects, particularly with regard to external (climate) versus internal (physiology) processes.

4.1 | Seasonal relationships obscured by seasonal lags

In this study, we used the autocorrelation function (ACF) and cross-correlation function (CCF) to assess the correlation between EW1 and LW for $\delta^{13}C$ and $\delta^{18}O$ chronologies. ACF and CCF are routinely used in time series analysis to detect and remove temporal persistence on the basis of autoregressive modeling (Bloomfield, 2000; Bunn, 2008; Ghil et al., 2002; Holmes, 1992; Yamaguchi, 1986). Persistence is when a temporal system remains in the same departure sign (above or below the long-term mean) for more than one consecutive observation. Persistence refers to a time series that is positively autocorrelated across sequentially sampled points (Bloomfield, 2000; Ghil et al., 2002; Yamaguchi, 1986). We observed high-order and low-frequency autocorrelation in the EW1 fraction for $\delta^{13}C$ that lasted for 7–10 years at some sites (e.g., SLS, MVP, RCP), and for $\delta^{18}O$ that lasted for 10 years at some sites (e.g., WCP and RCP) mainly explained by a strong long-term trend. Low frequency in tree-ring time series has been attributed to external factors such as long-term climatic variations, progressive age effects on trees, and long-term responses to ecosystem disturbance (Cook, Meko, & Stockton, 1997; LaMarche, 1974; Lorimer, 1989). We hypothesize that the low-frequency influence in our study is distinct in cause from the higher frequency 2- to 3-year autocorrelation that we observed, with the latter due to internal factors such as the utilization of common nutrient or carbohydrate reserves, and the time-dependence of stress-repair processes such as restoration of xylem conductivity and replacement of lost leaf area (Adams et al., 2017; Anderegg et al., 2015; Hacke, Stiller, Sperry, Pittermann, & McCulloh, 2001; Timofeeva et al., 2017). In our study, ACF and CCF revealed a general positive autocorrelation structure, particularly in $\delta^{13}C$ chronologies. For some sites, with the highest-order ACFs in EW1 $\delta^{13}C$ values (e.g., SLS, MVP and RCP), positive autocorrelation may also reflect temporal trends associated with successive occurrence of anomalous droughts through several sequential years, a pattern which has impacted this part of the United States for the last few decades (Breshears et al., 2005; Williams et al., 2013). This hypothesis is supported in our analysis by the divergent trend between the expected and observed $\Delta^{13}C$ values (Figure 3). Where all sites in our study region show a reduction in $^{13}C/^{12}C$ fractionation, which is consistent with the general influence of a "drying" regional climate that fosters higher iWUE (lower c_i/c_a) compared to the numerous tree species used in the comprehensive analysis of Voelker et al. (2016).

The autocorrelation structure was conspicuous in trees from multiple sites across the NAM climate gradient and best seen in the EW1 fraction, suggesting that this low-frequency component is more likely coupled to synoptic, widespread (and potentially cyclic) climatic influences on winter precipitation, rather than variance in the cross-gradient influences of the NAM. Our observations of a clear and general autocorrelation in the $\delta^{13}C$ of EW1 and LW suggest that the common seasonal low-frequency component of the climate signal (Carrillo, Castro, Woodhouse, & Griffin, 2015) is detected in the iWUE expressed during the respective spring and summer seasons of active carbon assimilation. These conclusions on the shared autocorrelation in partial ring widths are similar to those derived in previous studies using partial ring width chronologies (Carrillo et al., 2015; Griffin et al., 2013). The

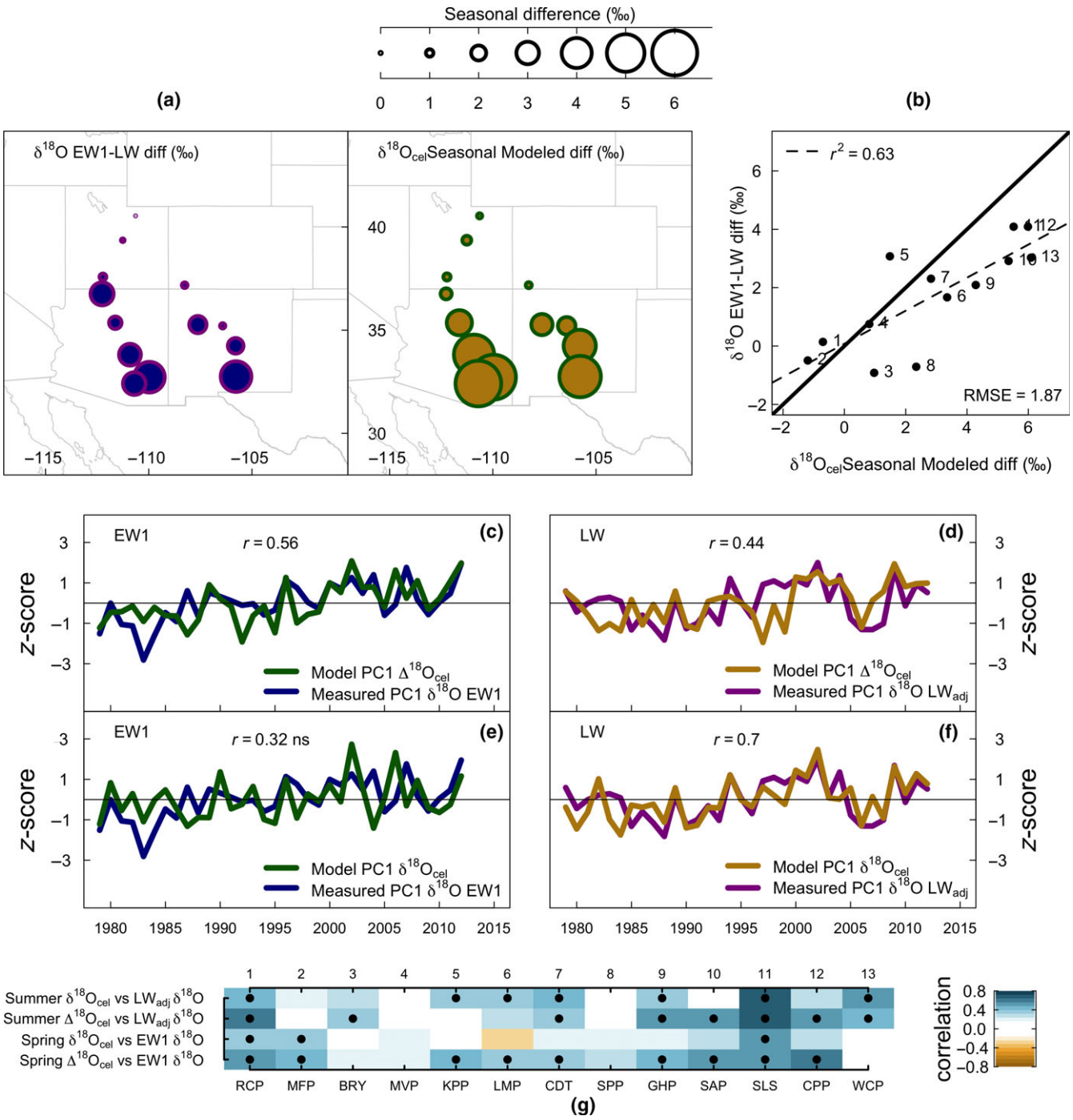

FIGURE 7 Consistency of the observed difference of $\delta^{18}O$ ratios, and $\Delta^{18}O$ ratios, between EW1 and LW with the difference modeled by a coupled isotope–climate model. (a) Mean annual difference in seasonal isotope ratios at individual sites for observed (left map) and modeled (right map) values. (b) Scatterplot of observed and modeled $\delta^{18}O$ differences, solid line represents 1:1 relationship, where modeled = observed, and the dashed line is the least square regression between observed and modeled $\delta^{18}O$ EW1-LW differences. (c) *z*-score time plots of the EW1 observed $\delta^{18}O$ and the EW1 modeled $\Delta^{18}O_{cel}$ (r = 0.56). (d) *z*-score plots of the observed LW_{adj} $\delta^{18}O$ and the modeled LW $\Delta^{18}O_{cel}$ (r = 0.44). (e–f) *z*-score time plots of the observed versus modeled $\delta^{18}O$ for EW1 (r = 0.32) and LW_{adj} (r = 0.7). Isotopic differences in the maps are coded by symbol size according to the key at the top of figure. Subscript "cel" denotes "cellulose" and identifies model results, as opposed to measurements in EW1 and LW. Pearson correlation values (r) between modeled and observed isotopes are reported in each plot. (g) Site based comparison between modeled and observed oxygen isotope ratios. The color code is the Pearson correlation coefficients between temporal variability of the modeled $\delta^{18}O_{cel}$ and $\Delta^{18}O_{cel}$ with the temporal variability of the $\delta^{18}O$ EW1 and LWadj measurements. Significant values ($p < 0.05$) are highlighted in bold point

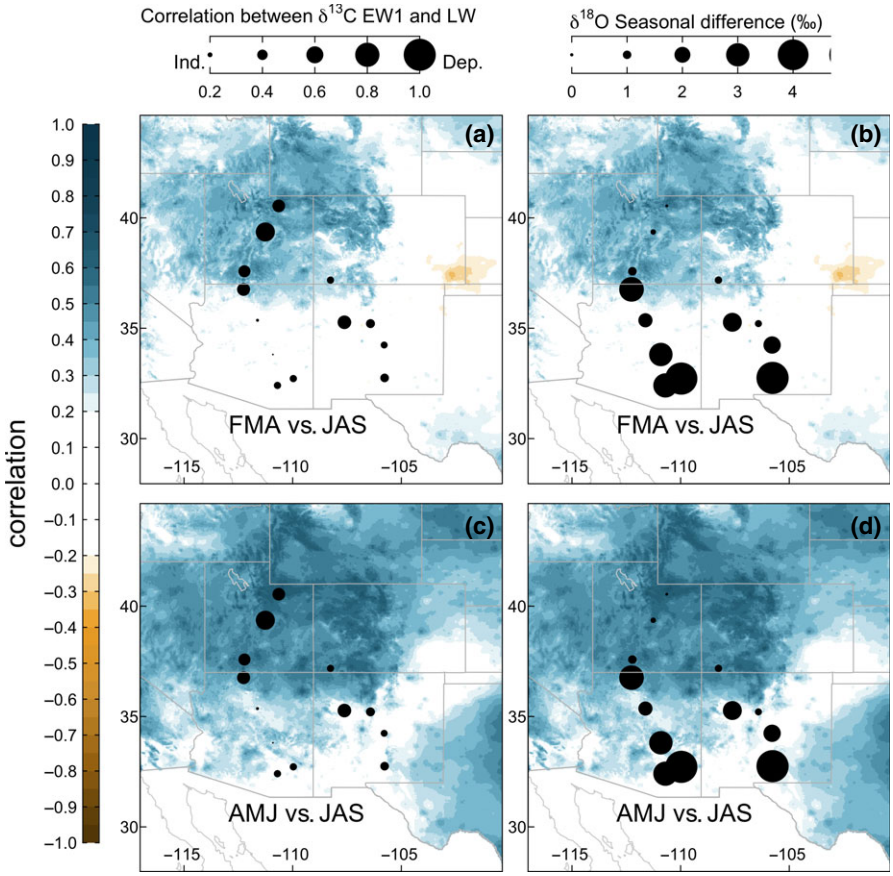

FIGURE 8 Interseason correlations of VPD (1960–2012) and interseasonal relationships of subannual isotope series. Shading is color-coded field correlation of VPD for the annotated 3-month seasons of February–April (FMA), April–June (AMJ), and July–September (JAS). Circles in the left maps (a, c) code the interseason (EW1 vs LW) correlation of $\delta^{13}C$. Circles in the right maps (b, d) code the interseason difference (EW1-LW) of $\delta^{18}O$. Circles are sized according to the keys shown above the maps. Note that circle-patterns in c and d are identical to those in (a) and (b)

low-frequency variability in $\delta^{13}C$ in both EW1 and LW was also detected with the CCF, showing significant positive correlations from negative to positive lags LW_{t-1}, $EW1_t$, LW_t, and $EW1_{t+1}$ (Figure 4).

After filtering the autocorrelation from LW and EW1 isotope chronologies, the strength of the interseasonal cross-correlations between LW on EW1 isotope chronologies decreased, but their presence persisted (Figure 8). These residual correlations most likely reflect higher-frequency effects, such as the common utilization of stored carbohydrate pools or stored soil water pools within the same year. The common use of resources would introduce interseasonal lags in the influence of climate on observed patterns in iWUE, g_s and A (Helle & Schleser, 2004; Kimak & Leuenberger, 2015; Kress et al., 2009; Labotka et al., 2016; Leavitt, 2010; Sargeant & Singer, 2016; Vaganov et al., 2009). The linear regression approach that we applied to the EW1 and LW time series was effective in distinguishing sites that show clear evidence of seasonal dependence of isotope ratios on climate. This finding was seen in the fact that the variance of the $\delta^{13}C$ LW chronologies showed a significant signal from the combined influences of both spring and summer VPD, whereas the variance of the corrected $\delta^{13}C$ LW_{adj} chronologies (see Materials and Methods) excluded the spring VPD signal and retained only summer-related variability, especially in the southern sites that lie within the core of the NAM climate system (Figure 6).

4.2 | Geographical patterns in the isotope variability in EW and LW

It is theoretically possible that interseasonal influences, such as those shown in Figure 8, can be caused by extrinsic factors, such as large-scale geospatial climate trends and teleconnections (i.e., large-scale causal relationships in climate) that cause winter and summer precipitation regimes to be positively correlated at specific sites. This could occur, for example, for EW1 and LW $\delta^{13}C$ if dry springs are followed by dry summers, both of which would be correlated with higher $\delta^{13}C_{cel}$. However, past studies, if they report the existence of cross-correlation in successive-season precipitation patterns, have reported negative, not positive, correlations (Grimm, Pal, & Giorgi, 2007; Kim, Kim, Arritt, & Miller, 2002). As a specific example, Castro, McKee, and Pielke (2001), Castro, Pielke, Adegoke, Schubert, and Pegion (2007) showed that during cool phases of El Niño Southern Oscillation (ENSO) and the Pacific Decadal Variability, winter precipitation in the western United States is generally below average, but the subtropical ridge is displaced further north than usual during the early summer, causing earlier and stronger monsoon activity in the arid southwestern United States. Bieda, Castro, Mullen, Comrie, and Pytlak (2009) supported these results, showing that cooler sea surface temperature (SST) in the Eastern Pacific favors more frequent occurrence and northward tracking of summertime upper-level disturbances that cause more frequent-than-normal bursts of summer

monsoon rainfall. In contrast, Griffin et al. (2013) reconstructed 500 years of cool- and warm-season standardized precipitation index from EW and LW ring widths and found that the previously reported antecedent negative correlations are not temporally stable when considered across longer centennial timescales, especially in the US NAM region. Thus, while there is some room for uncertainty, several analyses of observational data—supported by modeling—suggest that over the past ca. 100 years wet (dry) winters can be followed by dry (wet) monsoons, and this negative correlation may be caused by temporal and spatial connections involving mountain snowpack albedo, remote Pacific Ocean SST, and greenhouse gas forcing of the surface radiative balance (Cook & Seager, 2013; Grantz, Rajagopalan, Clark, & Zagona, 2007; Gutzler & Preston, 1997). The existence of a negative correlation in the seasonal precipitation of winter versus summer would work in the opposite direction to that required for explaining the general and positive cross-correlations in the isotope signals of EW1 and LW in our analysis. There are, however, some nuanced exceptions in these seasonal weather (VPD) relationships, depending on specific season and geographic regions (Figure 8).

We observed a clear increasing trend of seasonal cross-correlation in the $\delta^{13}C$ in EW1 and LW from south to north, following the gradient of decreasing summer monsoon influence (Figure 8). In the southernmost sites, which are characterized by distinct bimodal seasonality related to the NAM, we observed less dependence of LW $\delta^{13}C$ on EW1, than in the northernmost sites. This spatial trend was evident even after removal of the low-frequency autocorrelation (Figure 5c,f), indicating the presence of intra-annual, differential winter and summer influences between the EW1 and LW isotope signals. These patterns were less obvious for $\delta^{18}O$. It is not clear why significant intra-annual correlations are less frequently observed in $\delta^{18}O$ of EW1 and LW, compared to $\delta^{13}C$. It is possible that commonly used carbohydrate stores influences $\delta^{13}C$ more than $\delta^{18}O$. It is also possible that the potential for secondary isotope exchanges with nonfractionated xylem water for $\delta^{18}O$ during xylogenesis, explains the contrasting patterns for $\delta^{13}C$ and $\delta^{18}O$; both processes would potentially decrease distinctions in $\delta^{18}O$ between EW1 and LW.

Once the cross-correlations were removed from the intraseasonal components of the time series, thereby creating discrete seasonal time series, we were able to more accurately assess the direct influences of summer precipitation, and associated reduced VPD, on the isotopic composition of the LW_{adj}. As previously reported, there are clear differential influences of summer climate on the $\delta^{13}C$ and $\delta^{18}O$ of LW (Labotka et al., 2016; Sargeant & Singer, 2016; Treydte et al., 2014). Consistent with previously reported observations, in this region, VPD has a particularly strong influence on LW cellulose isotope ratios (Szejner et al., 2016). Reduced VPD on most days in the core of the NAM domain, during late-summer, in combination with the seasonal recharge of soil water stores, presumably foster higher steady-state ratios of intercellular-to-ambient CO_2 concentration (c_i/c_a), which reflect lower needle intrinsic water-use efficiency (iWUE) and isotope discrimination leading to lighter isotope ratios in both the $\delta^{13}C$ and $\delta^{18}O$ of tree-ring cellulose.

4.3 | Mechanistic interpretation of $\delta^{18}O$ EW and $\delta^{18}O$ LW under seasonal climate variations

We deployed a mechanistic model (Barbour et al., 2004; Roden et al., 2000) to better inform us of the causes of the observed spatial pattern in the seasonal differences between the $\delta^{18}O$ values in EW1 and LW. Using the model, we documented significant relationships between our observations of $\delta^{18}O$ in EW1 and the modeled results of $\Delta^{18}O_{cel}$ for spring (Figure 7). In the case of modeled $\Delta^{18}O_{cel}$ values, "Δ" refers to enrichment alone and does not include variations in source water $\delta^{18}O$ (Barbour et al., 2004). In the case of modeled $\delta^{18}O_{cel}$ values, however, "δ" refers to enrichment plus the seasonally varying source water isotope fraction (Cheesman & Cernusak, 2016; Gessler et al., 2014; Offermann et al., 2011). Our modeled results suggest that the most important determinant of the temporal variability in the observed $\delta^{18}O$ of EW1 across the geographic gradient is enrichment, driven by VPD and the associated evaporative fractionation effect, rather than variation in the isotopic composition of source water. In applying this same modeling approach for the observed $\delta^{18}O$ values of LW, we found that both modeled $\delta^{18}O_{cel}$ and $\Delta^{18}O_{cel}$ show significant relationships with observed LW_{adj} $\delta^{18}O$ (Figure 7), and inclusion of source water in the model ($\delta^{18}O_{cel}$) more than doubles the variance explained. This pattern in the LW_{adj} $\delta^{18}O$ suggests that monsoon reduction in the VPD has a significant role in reducing evaporative enrichment, such that variability in the source water $\delta^{18}O$ becomes evident as a larger component explaining the total observed variance in $\delta^{18}O_{cel}$.

Our studies have shown significant cross-correlations between isotope ratios in EW1 and LW, with low-frequency and high-frequency components are amenable to independent partitioning. The magnitude of these potentially confounding cross-correlations varies geographically, as evidenced in our observations across a prominent gradient in the contribution of summer precipitation. The existence of subannual connections is itself informative as to the effect of seasonal and multi-year lags on isotopic variance. Once the cross-correlations were identified, we could implement a statistical correction to account for confounding effects in our search for seasonal isotope–climate-physiology linkages. Once corrected, we were able to use mechanistic modeling to predict the $\delta^{18}O$ in cellulose and show that VPD played a dominant role in driving the observed EW1 $\delta^{18}O$ variance. In contrast, both VPD and source water had significant influences on the $\delta^{18}O$ of LW_{adj} across the entire geographic gradient. In general, our results show that it is possible to disentangle isotope ratio source mixing across intra-annual portions of tree rings. These findings allow us to gain insight into the phenology and lags associated with carbon assimilation, allocation to wood production and the differential utilization of winter versus summer precipitation in coupling the water and carbon cycles in these montane ecosystems. These insights should be especially useful in the exploration of past geographical shifts in the NAM climate system and of past temporal patterns in the climate variability that influences ecosystem productivity and water resource delivery in montane forests of the semi-arid southwestern US region.

ACKNOWLEDGEMENTS

This study was supported by grants from the Macrosystems Program in the Emerging Frontiers Section (NSF Award 1065790), the Ecosystems Program in the Division of Environmental Biology (NSF Award 1754430), and the Inter-University Training Program in Continental-scale Ecology (NSF award 1137336), all of which are administered within the U.S. National Science Foundation. We thank Elisabeth Bergman, Miles Twitty, Fred Moreno, Leon Prescott Wells, Monica Vogel, Megan Mckey, Grace Kim, Alyssa Langford Abbey, and Seth Stephens for their technical assistance. We thank Arthur Gessler for supporting this manuscript and Steve Voelker for his valuable input throughout the review process and two anonymous reviewers that helped improve the manuscript. The tree-ring data and isotope chronologies will be archived in the International Tree-Ring Databank or will be made available upon request to Paul Szejner (paulszejner@email.arizona.edu).

ORCID

Paul Szejner http://orcid.org/0000-0002-7780-1215

REFERENCES

Adams, H. D., Zeppel, M. J. B., Anderegg, W. R. L., Hartmann, H., Landhäusser, S. M., Tissue, D. T., … McDowell, N. G. (2017). A multi-species synthesis of physiological mechanisms in drought-induced tree mortality. *Nature Ecology & Evolution*, *1*, 1285–1291. https://doi.org/10.1038/s41559-017-0248-x

Anderegg, W. R. L., Schwalm, C. R., Biondi, F., Camarero, J. J., Koch, G., Litvak, M., … Pacala, S. (2015). Pervasive drought legacies in forest ecosystems and their implications for carbon cycle models. *Science*, *349*, 528–532. https://doi.org/10.1126/science.aab1833

Babst, F., Wright, W. E., Szejner, P., Wells, L., Belmecheri, S., & Monson, R. K. (2016). Blue intensity parameters derived from Ponderosa pine tree rings characterize intra-annual density fluctuations and reveal seasonally divergent water limitations. *Trees*, *30*, 1403–1415. https://doi.org/10.1007/s00468-016-1377-6

Bale, R. J., Robertson, I., Salzer, M. W., Loader, N. J., Leavitt, S. W., Gagen, M., … McCarroll, D. (2011). An annually resolved bristlecone pine carbon isotope chronology for the last millennium. *Quaternary Research*, *76*, 22–29. https://doi.org/10.1016/j.yqres.2011.05.004

Barbour, M. M., Roden, J. S., Farquhar, G. D., & Ehleringer, J. R. (2004). Expressing leaf water and cellulose oxygen isotope ratios as enrichment above source water reveals evidence of a Péclet effect. *Oecologia*, *138*, 426–435. https://doi.org/10.1007/s00442-003-1449-3

Barbour, M. M., Walcroft, A. S., & Farquhar, G. D. (2002). Seasonal variation in δ13C and δ18O of cellulose from growth rings of *Pinus radiata*. *Plant, Cell and Environment*, *25*, 1483–1499. https://doi.org/10.1046/j.0016-8025.2002.00931.x

Belmecheri, S., Wright, W. E., Szejner, P., Morino, K. A., & Monson, R. K. (2018). Carbon and oxygen isotope fractionations in tree rings reveal interactions between cambial phenology and seasonal climate. *Plant, Cell & Environment* (in press). https://doi.org/10.1111/pce.13401

Berkelhammer, M., Stefanescu, I. C., Joiner, J., & Anderson, L. (2017). High sensitivity of gross primary production in the Rocky Mountains to summer rain. *Geophysical Research Letters*, *44*, 3643–3652. https://doi.org/10.1002/2016GL072495

Betancourt, J. L. (1990). Late quaternary biogeography of the Colorado Plateau. In J. L. Betancourt, T. R. van Devender & P. S. Martin (Eds.), *Packrat middens: The last 40,000 years of biotic change* (pp. 259–292). Tucson, AZ: University of Arizona Press.

Bhattacharya, T., Tierney, J. E., & DiNezio, P. (2017). Glacial reduction of the North American Monsoon via surface cooling and atmospheric ventilation. *Geophysical Research Letters*, *44*, 5113–5122. https://doi.org/10.1002/2017GL073632

Bieda, S. W., Castro, C. L., Mullen, S. L., Comrie, A. C., & Pytlak, E. (2009). The relationship of transient upper-level troughs to variability of the North American monsoon system. *Journal of Climate*, *22*, 4213–4227. https://doi.org/10.1175/2009JCLI2487.1

Bloomfield, P. (2000). *Fourier analysis of time series*. Hoboken, NJ: John Wiley & Sons Inc. https://doi.org/10.1002/0471722235

Breshears, D. D., Cobb, N. S., Rich, P. M., Price, K. P., Allen, C. D., Balice, R. G., … Meyer, C. W. (2005). Regional vegetation die-off in response to global-change-type drought. *Proceedings of the National Academy of Sciences USA*, *102*, 15144–15148. https://doi.org/10.1073/pnas.0505734102

Bunn, A. G. (2008). A dendrochronology program library in R (dplR). *Dendrochronologia*, *26*, 115–124. https://doi.org/10.1016/j.dendro.2008.01.002

Carrillo, C. M., Castro, C. L., Woodhouse, C. A., & Griffin, D. (2015). Low-frequency variability of precipitation in the North American monsoon region as diagnosed through earlywood and latewood tree-ring chronologies in the southwestern US. *International Journal of Climatology*, *36*, 2254–2272.

Castro, C. L., McKee, T. B., & Pielke, R. A. (2001). The relationship of the North American monsoon to tropical and North Pacific sea surface temperatures as revealed by observational analyses. *Journal of Climate*, *14*, 4449–4473. https://doi.org/10.1175/1520-0442(2001)014<4449:TROTNA>2.0.CO;2

Castro, C. L., Pielke, R. A., Adegoke, J. O., Schubert, S. D., & Pegion, P. J. (2007). Investigation of the summer climate of the contiguous United States and Mexico using the Regional Atmospheric Modeling System (RAMS). Part II: Model climate variability. *Journal of Climate*, *20*, 3866–3887. https://doi.org/10.1175/JCLI4212.1

Cernusak, L. A., Barbour, M. M., Arndt, S. K., Cheesman, A. W., English, N. B., Feild, T. S., … Farquhar, G. D. (2016). Stable isotopes in leaf water of terrestrial plants. *Plant, Cell & Environment*, *39*, 1087–1102. https://doi.org/10.1111/pce.12703

Cheesman, A. W., & Cernusak, L. A. (2016). Infidelity in the outback: Climate signal recorded in Δ18O of leaf but not branch cellulose of eucalypts across an Australian aridity gradient. *Tree Physiology*, *37*, 554–564.

Cook, E. R., Meko, D. M., & Stockton, C. W. (1997). A new assessment of possible solar and lunar forcing of the bidecadal drought rhythm in the Western United States. *Journal of Climate*, *10*, 1343–1356. https://doi.org/10.1175/1520-0442(1997)010<1343:ANAOPS>2.0.CO;2

Cook, B. I., & Seager, R. (2013). The response of the North American Monsoon to increased greenhouse gas forcing. *Journal of Geophysical Research: Atmospheres*, *118*, 1690–1699.

Craig, H. (1954). Carbon-13 variations in Sequoia rings and the atmosphere. *Science*, *119*, 141–144. https://doi.org/10.1126/science.119.3083.141

Craig, H., & Gordon, L. (1965). Deuterium and oxygen 18 variations in the ocean and the marine atmosphere. In E. Tongiorgi (Ed.), *Stable Isotopes in Oceanographic Studies and Paleotemperatures* (pp. 9–130). Pisa, Italy: Consiglio Nazionale delle ricerche Laboratorio di Geologia Nucleare.

Ehleringer, J. R., & Cerling, T. E. (1995). Atmospheric CO_2 and the ratio of intercellular to ambient CO_2 concentrations in plants. *Tree Physiology*, *15*, 105–111. https://doi.org/10.1093/treephys/15.2.105

Farquhar, G. D., & Cernusak, L. A. (2005). On the isotopic composition of leaf water in the non- steady state. *Functional Plant Biology*, *32*, 293–303.

Farquhar, G. D., Cernusak, L. A., & Barnes, B. (2007). Heavy water fractionation during transpiration. *Plant Physiology*, *143*, 11–18.

Farquhar, G., Ehleringer, J., & Hubick, K. (1989). Carbon isotope discrimination and photosynthesis. *Annual Review of Plant Physiology*, *40*, 503–537. https://doi.org/10.1146/annurev.pp.40.060189.002443

Farquhar, G. D., Lloyd, J., Taylor, J. A., Flanagan, L. B., Syvertsen, J. P., Hubick, K. T., … Ehleringer, J. R. (1993). Vegetation effects on the isotope composition of oxygen in atmospheric CO_2. *Nature*, *363*, 439–443. https://doi.org/10.1038/363439a0

Farquhar, G. D., Oleary, M. H., & Berry, J. A. (1982). On the relationship between carbon isotope discrimination and the Inter-cellular carbon-dioxide concentration in leaves. *Australian Journal of Plant Physiology*, *9*, 121–137. https://doi.org/10.1071/PP9820121

Ficklin, D. L., & Novick, K. A. (2017). Historic and projected changes in vapor pressure deficit suggest a continental-scale drying of the United States atmosphere. *Journal of Geophysical Research: Atmospheres*, *122*, 2061–2079.

Francey, R., & Farquhar, G. (1982). An explanation of 13C/12C variations in tree rings. *Nature*, *297*, 28–31. https://doi.org/10.1038/297028a0

Frank, D. C., Poulter, B., Saurer, M., Esper, J., Huntingford, C., Helle, G., … Weigl, M. (2015). Water-use efficiency and transpiration across European forests during the Anthropocene. *Nature Climate Change*, *5*, 579–583. https://doi.org/10.1038/nclimate2614

Fritts, H. C. (1976). *Tree rings and climate* (pp. 567, Vol. 226). Caldwell, NJ: The Blackburn Press.

Gessler, A., Ferrio, J. P., Hommel, R., Treydte, K., Werner, R. A., & Monson, R. K. (2014). Stable isotopes in tree rings: Towards a mechanistic understanding of isotope fractionation and mixing processes from the leaves to the wood. *Tree Physiology*, *34*, 796–818. https://doi.org/10.1093/treephys/tpu040

Ghil, M., Allen, M. R., Dettinger, M. D., Ide, K., Kondrashov, D., Mann, M. E., … Yiou, P. (2002). Advanced spectral methods for climate time series. *Reviews of Geophysics*, *40*, 3.1–3.41.

Grantz, K., Rajagopalan, B., Clark, M., & Zagona, E. (2007). Seasonal shifts in the North American monsoon. *Journal of Climate*, *20*, 1923–1935. https://doi.org/10.1175/JCLI4091.1

Griffin, D., Meko, D. M., Touchan, R., Leavitt, S. W., & Woodhouse, C. A. (2011). Latewood chronology development for summer-moisture reconstruction in the US southwest. *Tree-Ring Research*, *67*, 87–101. https://doi.org/10.3959/2011-4.1

Griffin, D., Woodhouse, C. A., Meko, D. M., Stahle, D. W., Faulstich, H. L., Carrillo, C., … Leavitt, S. W. (2013). North American monsoon precipitation reconstructed from tree-ring latewood. *Geophysical Research Letters*, *40*, 954–958. https://doi.org/10.1002/grl.50184

Grimm, A. M., Pal, J. S., & Giorgi, F. (2007). Connection between spring conditions and peak summer monsoon rainfall in South America: Role of soil moisture, surface temperature, and topography in eastern Brazil. *Journal of Climate*, *20*, 5929–5945. https://doi.org/10.1175/2007JCLI1684.1

Gutzler, D. S., & Preston, J. W. (1997). Evidence for a relationship between spring snow cover in North America and summer rainfall in New Mexico. *Geophysical Research Letters*, *24*, 2207–2210. https://doi.org/10.1029/97GL02099

Hacke, U. G., Stiller, V., Sperry, J. S., Pittermann, J., & McCulloh, K. A. (2001). Cavitation fatigue. Embolism and refilling cycles can weaken the cavitation resistance of xylem. *Plant physiology*, *125*, 779–786. https://doi.org/10.1104/pp.125.2.779

Helle, G., & Schleser, G. H. (2004). Beyond CO_2-fixation by Rubisco – An interpretation of 13C/12C variations in tree rings from novel intra-seasonal studies on broad-leaf trees. *Plant, Cell and Environment*, *27*, 367–380. https://doi.org/10.1111/j.0016-8025.2003.01159.x

Higgins, R. W., Yao, Y., & Wang, X. L. (1997). Influence of the North American monsoon system on the U.S. summer precipitation regime. *Journal of Climate*, *10*, 2600–2622. https://doi.org/10.1175/1520-0442(1997)010<2600:IOTNAM>2.0.CO;2

Holmes, R. L. (1992). Dendrochronology Program Library, Instruction and Program Manual (January 1992 update).

Hu, J., Moore, D. J. P., Burns, S. P., & Monson, R. (2010). Longer growing seasons lead to less carbon sequestration by a subalpine forest. *Global Change Biology*, *16*, 771–783. https://doi.org/10.1111/j.1365-2486.2009.01967.x

Jenkins, G. M., & Watts, D. G. (1968). *Spectral analysis and its applications*. Boca Raton, FL: Holden-Day.

Kagawa, A., Sugimoto, A., & Maximov, T. C. (2006). Seasonal course of translocation, storage and remobilization of 13C pulse-labeled photoassimilate in naturally growing *Larix gmelinii* saplings. *New Phytologist*, *171*, 793–804. https://doi.org/10.1111/j.1469-8137.2006.01780.x

Kerhoulas, L., Kolb, T., & Koch, G. (2017). The influence of monsoon climate on latewood growth of southwestern ponderosa pine. *Forests*, *8*, 140. https://doi.org/10.3390/f8050140

Kim, J., Kim, T.-K., Arritt, R. W., & Miller, N. L. (2002). Impacts of increased atmospheric CO_2 on the hydroclimate of the Western United States. *Journal of Climate*, *15*, 1926–1942. https://doi.org/10.1175/1520-0442(2002)015<1926:IOIACO>2.0.CO;2

Kimak, A., & Leuenberger, M. (2015). Are carbohydrate storage strategies of trees traceable by early–latewood carbon isotope differences? *Trees*, *29*, 859–870. https://doi.org/10.1007/s00468-015-1167-6

Kress, A., Young, G. H. F., Saurer, M., Loader, N. J., Siegwolf, R. T. W., & McCarroll, D. (2009). Stable isotope coherence in the earlywood and latewood of tree-line conifers. *Chemical Geology*, *268*, 52–57. https://doi.org/10.1016/j.chemgeo.2009.07.008

Labotka, D. M., Grissino-Mayer, H. D., Mora, C. I., & Johnson, E. J. (2016). Patterns of moisture source and climate variability in the southeastern United States: A four-century seasonally resolved tree-ring oxygen-isotope record. *Climate Dynamics*, *46*, 2145–2154. https://doi.org/10.1007/s00382-015-2694-y

LaMarche, V. C. (1974). Frequency-dependent relationships between tree-ring series along an ecological gradient and some dendroclimatic implications. *Tree-Ring Bulletin*, *34*, 1–20.

Leavitt, S. W. (2001). Response of δ13C in *Pinus resinosa* Ait. seedling secondary xylem tissue to changing environment in controlled growth experiments. *Dendrochronologia*, *19*, 9–22.

Leavitt, S. W. (2002). Spatial expression of ENSO, drought, and summer monsoon in seasonal δ 13 C of ponderosa pine tree rings in southern Arizona and New Mexico. *Journal of Geophysical Research*, *107*, 4349. https://doi.org/10.1029/2001JD001312

Leavitt, S. W. (2010). Tree-ring C-H-O isotope variability and sampling. *Science of the Total Environment*, *408*, 5244–5253. https://doi.org/10.1016/j.scitotenv.2010.07.057

Leavitt, S. W., & Danzer, S. R. (1993). Method for batch processing small wood samples to holocellulose for stable-carbon isotope analysis. *Analytical Chemistry*, *65*, 87–89. https://doi.org/10.1021/ac00049a017

Leavitt, S. W., & Long, A. (1986). Stable-carbon isotope variability in tree foliage and wood. *Ecology*, *67*, 1002–1010. https://doi.org/10.2307/1939823

Libby, L. M., & Pandolfi, L. J. (1974). Temperature dependence of isotope ratios in tree rings. *Proceedings of the National Academy of Sciences USA*, *71*, 2482–2486. https://doi.org/10.1073/pnas.71.6.2482

Lorimer, C. G. (1989). Relative effects of small and large disturbances on temperate hardwood forest structure. *Ecology*, *70*, 565–567. https://doi.org/10.2307/1940207

McCarroll, D., Gagen, M. H., Loader, N. J., Robertson, I., Anchukaitis, K. J., Los, S., … Waterhouse, J. S. (2009). Correction of tree ring stable carbon isotope chronologies for changes in the carbon dioxide

content of the atmosphere. *Geochimica et Cosmochimica Acta*, *73*, 1539–1547. https://doi.org/10.1016/j.gca.2008.11.041

McCarroll, D., & Loader, N. J. (2004). Stable isotopes in tree rings. *Quaternary Science Reviews*, *23*, 771–801. https://doi.org/10.1016/j.quascirev.2003.06.017

Meko, D. M., & Baisan, C. H. (2001). Pilot study of latewood-width of conifers as an indicator of variability of summer rainfall in the North American monsoon region. *International Journal of Climatology*, *21*, 697–708. https://doi.org/10.1002/(ISSN)1097-0088

Monson, R. K., Sparks, J. P., Rosenstiel, T. N., Scott-Denton, L. E., Huxman, T. E., Harley, P. C., … Hu, J. (2005). Climatic influences on net ecosystem CO_2 exchange during the transition from wintertime carbon source to springtime carbon sink in a high-elevation, subalpine forest. *Oecologia*, *146*, 130–147. https://doi.org/10.1007/s00442-005-0169-2

Offermann, C., Ferrio, J. P., Holst, J., Grote, R., Siegwolf, R., Kayler, Z., & Gessler, A. (2011). The long way down – Are carbon and oxygen isotope signals in the tree ring uncoupled from canopy physiological processes? *Tree Physiology*, *31*, 1088–1102. https://doi.org/10.1093/treephys/tpr093

Ogée, J., Barbour, M. M., Wingate, L., Bert, D., Bosc, A., Stievenard, M., … Dewar, R. C. (2009). A single-substrate model to interpret intra-annual stable isotope signals in tree-ring cellulose. *Plant, Cell and Environment*, *32*, 1071–1090. https://doi.org/10.1111/j.1365-3040.2009.01989.x

Pallardy, S. G. (2008). *Physiology of woody plants*. New York, NY: Elsevier.

Pellizzari, E., Camarero, J. J., Gazol, A., Sangüesa-Barreda, G., & Carrer, M. (2016). Wood anatomy and carbon-isotope discrimination support long-term hydraulic deterioration as a major cause of drought-induced dieback. *Global Change Biology*, *22*, 2125–2137. https://doi.org/10.1111/gcb.13227

PRISM_Climate_Group (2004). Oregon State University. PRISM.

Rahman, M. H., Begum, S., Nakaba, S., Yamagishi, Y., Kudo, K., Nabeshima, E., … Funada, R. (2016). Relationship between the earlywood-to-latewood transition and changes in levels of stored starch around the cambium in locally heated stems of the evergreen conifer *Chamaecyparis pisifera*. *Trees – Structure and Function*, *30*, 1619–1631. https://doi.org/10.1007/s00468-016-1395-4

Roden, J. S., & Ehleringer, J. R. (2007). Summer precipitation influences the stable oxygen and carbon isotopic composition of tree-ring cellulose in *Pinus ponderosa*. *Tree Physiology*, *27*, 491–501. https://doi.org/10.1093/treephys/27.4.491

Roden, J., Kahmen, A., Buchmann, N., & Siegwolf, R. (2015). The enigma of effective path length for 18 O enrichment in leaf water of conifers. *Plant, Cell & Environment*, *38*, 2551–2565. https://doi.org/10.1111/pce.12568

Roden, J., Lin, G., & Ehleringer, J. R. (2000). A mechanistic model for interpretation of hydrogen and oxygen isotope ratios in tree-ring cellulose. *Geochimica et Cosmochimica Acta*, *64*, 21–35. https://doi.org/10.1016/S0016-7037(99)00195-7

Sargeant, C. I., & Singer, M. B. (2016). Sub-annual variability in historical water source use by Mediterranean riparian trees. *Ecohydrology*, *9*, 1328–1345. https://doi.org/10.1002/eco.1730

Saurer, M., Robertson, I., Siegwolf, R., & Leuenberger, M. (1998). Oxygen isotope analysis of cellulose: An interlaboratory comparison. *Analytical Chemistry*, *70*, 2074–2080. https://doi.org/10.1021/ac971022f

Schimel, D., Kittel, T. G. F., Running, S., Monson, R., Turnipseed, A., & Anderson, D. (2002). Carbon sequestration studied in western U.S. mountains. *Eos, Transactions American Geophysical Union*, *83*, 445. https://doi.org/10.1029/2002EO000314

Sheppard, P. R., Comrie, A. C., Packin, G. D., Angersbach, K., & Hughes, M. K. (2002). The climate of the US southwest. *Climate Research*, *21*, 219–238. https://doi.org/10.3354/cr021219

Stahle, D. W., Cleaveland, M. K., Grissino-Mayer, H. D., Griffin, R. D., Fye, F. K., Therrell, M. D., … Villanueva Diaz, J. (2009). Cool- and warm-season precipitation reconstructions over Western New Mexico. *Journal of Climate*, *22*, 3729–3750. https://doi.org/10.1175/2008JCLI2752.1

Sternberg, L., & DeNiro, M. (1983). Biogeochemical implications of the isotopic equilibrium fractionation factor between the oxygen atoms of acetone and water. *Geochimica et Cosmochimica Acta*, *47*, 2271–2274. https://doi.org/10.1016/0016-7037(83)90049-2

Sternberg, L., & Ellsworth, P. F. V. (2011). Divergent biochemical fractionation, not convergent temperature, explains cellulose oxygen isotope enrichment across latitudes. *PLoS One*, *6*, e28040. https://doi.org/10.1371/journal.pone.0028040

Stokes, M. A., & Smiley, T. L. (1996). *An introduction to tree-ring dating* (pp. 73). Tucson, AZ: The University of Arizona Press.

Suess, H. E. (1955). Radiocarbon concentration in modern wood. *Science*, *122*, 415–417. https://doi.org/10.1126/science.122.3166.415-a

Szejner, P., Wright, W. E., Babst, F., Belmecheri, S., Trouet, V., Leavitt, S. W., … Monson, R. K. (2016). Latitudinal gradients in tree ring stable carbon and oxygen isotopes reveal differential climate influences of the North American Monsoon System. *Journal of Geophysical Research: Biogeosciences*, *121*, 1978–1991.

Szymczak, S., Joachimski, M. M., Bräuning, A., Hetzer, T., & Kuhlemann, J. (2012). A 560 yr summer temperature reconstruction for the Western Mediterranean basin based on stable carbon isotopes from *Pinus nigra* ssp. *laricio* (Corsica/France). *Climate of the Past*, *8*, 1737–1749. https://doi.org/10.5194/cp-8-1737-2012

Timofeeva, G., Treydte, K., Bugmann, H., Rigling, A., Schaub, M., Siegwolf, R., & Saurer, M. (2017). Long-term effects of drought on tree-ring growth and carbon isotope variability in Scots pine in a dry environment. *Tree Physiology*, *37*, 1028–1041. https://doi.org/10.1093/treephys/tpx041

Torbenson, M. C. A., Stahle, D. W., Villanueva Díaz, J., Cook, E. R., & Griffin, D. (2016). The relationship between earlywood and latewood ring-growth across North America. *Tree-Ring Research*, *72*, 53–66. https://doi.org/10.3959/1536-1098-72.02.53

Treydte, K., Boda, S., Graf Pannatier, E., Fonti, P., Frank, D., Ullrich, B., … Gessler, A. (2014). Seasonal transfer of oxygen isotopes from precipitation and soil to the tree ring: Source water versus needle water enrichment. *New Phytologist*, *202*, 772–783. https://doi.org/10.1111/nph.12741

Treydte, K., Frank, D., Esper, J., Andreu, L., Bednarz, Z., Berninger, F., … Schleser, G. H. (2007). Signal strength and climate calibration of a European tree-ring isotope network. *Geophysical Research Letters*, *34*, 2–7.

Vaganov, E. A., Schulze, E.-D., Skomarkova, M. V., Knohl, A., Brand, W. A., & Roscher, C. (2009). Intra-annual variability of anatomical structure and δ13C values within tree rings of spruce and pine in alpine, temperate and boreal Europe. *Oecologia*, *161*, 729–745. https://doi.org/10.1007/s00442-009-1421-y

van der Sleen, P., Zuidema, P. A., & Pons, T. L. (2017). Stable isotopes in tropical tree rings: Theory, methods and applications. *Functional Ecology*, *31*, 1674–1689. https://doi.org/10.1111/1365-2435.12889

Voelker, S. L., Brooks, J. R., Meinzer, F. C., Anderson, R., Bader, M. K.-F., Battipaglia, G., … Wingate, L. (2016). A dynamic leaf gas-exchange strategy is conserved in woody plants under changing ambient CO_2: Evidence from carbon isotope discrimination in paleo and CO_2 enrichment studies. *Global Change Biology*, *22*, 889–902. https://doi.org/10.1111/gcb.13102

Walcroft, A. S., Silvester, W. B., Whitehead, D., & Kelliher, F. M. (1997). Seasonal changes in stable carbon isotope ratios within annual rings of *Pinus radiata* reflect environmental regulation of growth processes. *Australian Journal of Plantphysiology*, *24*, 57–68. https://doi.org/10.1071/PP96025

West, A. G., Hultine, K. R., Burtch, K. G., & Ehleringer, J. R. (2007). Seasonal variations in moisture use in a piñon-juniper woodland. *Oecologia*, *153*, 787–798. https://doi.org/10.1007/s00442-007-0777-0

Williams, P. A., Allen, C. D., Macalady, A. K., Griffin, D., Woodhouse, C. A., Meko, D. M., … McDowell, N. G. (2013). Temperature as a potent driver of regional forest drought stress and tree mortality. *Nature Climate Change*, *3*, 292–297. https://doi.org/10.1038/nclimate1693

Winchell, T. S., Barnard, D. M., Monson, R. K., Burns, S. P., & Molotch, N. P. (2016). Earlier snowmelt reduces atmospheric carbon uptake in midlatitude subalpine forests. *Geophysical Research Letters*, *43*, 8160–8168. https://doi.org/10.1002/2016GL069769

Wright, W. E., & Leavitt, S. W. (2006). Boundary layer humidity reconstruction for a semiarid location from tree ring cellulose δ18O. *Journal of Geophysical Research: Atmospheres*, *111*, 1–9.

Yamaguchi, D. K. (1986). Interpretation cross correlation tree ring series. *Tree-Ring Bulletin*, *46*, 47–54.

Yoshimura, K., Kanamitsu, M., Noone, D., & Oki, T. (2008). Historical isotope simulation using Reanalysis atmospheric data. *Journal of Geophysical Research: Atmospheres*, *113*, 1–15.

Zapata-Rios, X., Brooks, P. D., Troch, P. A., McIntosh, J., & Rasmussen, C. (2016). Influence of climate variability on water partitioning and effective energy and mass transfer in a semi-arid critical zone. *Hydrology and Earth System Sciences*, *20*, 1103–1115. https://doi.org/10.5194/hess-20-1103-2016

Ziaco, E., Truettner, C., Biondi, F., & Bullock, S. (2018). Moisture-driven xylogenesis in *Pinus ponderosa* from a Mojave Desert mountain reveals high phenological plasticity. *Plant, Cell & Environment*, *41*, 823–836. https://doi.org/10.1111/pce.13152

SUPPORTING INFORMATION

Additional supporting information may be found online in the Supporting Information section at the end of the article.

How to cite this article: Szejner P, Wright WE, Belmecheri S, et al. Disentangling seasonal and interannual legacies from inferred patterns of forest water and carbon cycling using tree-ring stable isotopes. *Glob Change Biol*. 2018;00:1–16. https://doi.org/10.1111/gcb.14395